Remote Sensing of Environment 128 (2013) 234–245

Contents lists available at SciVerse ScienceDirect

Remote Sensing of Environment

journal homepage: www.elsevier.com/locate/rse

Aerosol optical depth retrieval in the Arctic region using MODIS data over snow

Linlu Mei [a,g,h], Yong Xue [b,c,*], Gerrit de Leeuw [d,e,f], Wolfgang von Hoyningen-Huene [g], Alexander A. Kokhanovsky [g], Larysa Istomina [g], Jie Guang [a], John P. Burrows [g]

[a] State Key Laboratory of Remote Sensing Science, Jointly Sponsored by the Institute of Remote Sensing Applications of Chinese Academy of Sciences and Beijing Normal University, Institute of Remote Sensing Applications, Chinese Academy of Sciences, Beijing 100101, China
[b] Center for Earth Observation and Digital Earth of Chinese Academy of Sciences, Beijing 100094, China
[c] Faculty of Computing, London Metropolitan University, 166-220 Holloway Road, London N7 8DB, UK
[d] Department of Physics, University of Helsinki, Helsinki, Finland
[e] Finnish Meteorological Institute, Climate Change Unit, Helsinki, Finland
[f] Netherlands Organisation for Applied Scientific Research TNO, Utrecht, the Netherlands
[g] Institute of Environmental Physics, University of Bremen, Otto-Hahn-Allee 1, 28359 Bremen, Germany
[h] University of the Chinese Academy of Sciences, Beijing 100049, China

ARTICLE INFO

Article history:
Received 31 March 2012
Received in revised form 12 October 2012
Accepted 13 October 2012
Available online 9 November 2012

Keywords:
Arctic region
Satellite remote sensing
Aerosol optical depth
Snow
Prior knowledge

ABSTRACT

The Arctic is vulnerable to the long-term transport of aerosols because they affect the surface albedo when particles are deposited on snow and ice. However, aerosol observations for this area are sparse and hence there is considerable uncertainty in the knowledge on the properties of the Arctic aerosol. Atmospheric remote sensing using satellite-based instruments offers an opportunity to obtain information on aerosol properties, in particular the aerosol optical depth (AOD) on an extended spatial scale as determined by the instrument's swath width. However, AOD retrieval over a bright surface is a difficult task because it is difficult to separate and explicitly describe the contribution of the surface and that due to back-scattering by aerosols to the radiance observed by a satellite at the top of the atmosphere (TOA), especially at large Solar Zenith Angles (SZA). In this paper, an approach to achieve this is presented based on a synergetic approach using data from both Moderate Resolution Imaging Spectroradiometer (MODIS) instruments flying on the TERRA and AQUA satellites. The approached also uses prior knowledge for aerosol properties retrieval over snow as well as a Snow Bidirectional Reflectance Distribution Function (BRDF) model. The detailed analysis of the model results demonstrates that the Aerosol Properties Retrieval over Snow (APRS) algorithm is suitable for Arctic region Aerosol Optical Depth (AOD) retrieval. The study periods include April 2010 and April 2011, when the Arctic haze mostly occurs. Six AERONET stations at high latitude (Andenes, Barrow, Ittoqqortoormiit, OPAL, Thule, and PEARL) were used for comparison. The correlation coefficient between retrieved AODs and AERONET AODs was 0.8 and the relative error is between 10% and 20%, demonstrating the potential of the APRS method to retrieve AOD over the Arctic, with highly reflective snow/ice surfaces and large solar zenith angles.

1. Introduction

The balance between greenhouse warming and aerosol cooling is an important issue in the discussion of global climate change (Kondratyev & Varotsos, 1995). Ocean warming has been reported to be delayed due to aerosol scattering of solar radiation (Delworth et al., 2005) while Shindell and Faluvegi (2009) suggested that aerosol may drive a significant portion of Arctic warming. The Arctic environment is a significant indicator of global change. Satellite observations and Lidar measurements have revealed the occurrence of substantial amounts of smoke and other particulate matter in the tropopause region and lower stratosphere at high latitudes and in the Arctic region (Damoah et al., 2004) due to transport of anthropogenic (Shaw, 1995) or natural aerosol produced by sources such as wildfires (Kim et al., 2005) and volcanic eruptions (Herber et al., 1996). Long-range transport over continental, intercontinental and even global distances is the dominant pollution source in the Arctic region (Stohl, 2006). The Arctic haze in spring (Ackerman et al., 1986) and biomass burning during summer play predominant roles in both the distribution of solar radiation and the total energy balance in the Arctic. Research to better understand changes in atmospheric composition and climate in the Arctic is urgently needed.

Ground-based observation is the primary method used for providing information on atmospheric composition in the Arctic. Aerosol property analysis using ground-based measurements has been done for certain Arctic regions such as Scandinavia and Svalbard (Toledano et al.,

* Corresponding author at: Faculty of Computing, London Metropolitan University, 166-220 Holloway Road, London N7 8DB, UK. Tel.: +44 1223 842644; fax: +44 20 71337053.
E-mail addresses: meilinlu@163.com (L. Mei), yx9@hotmail.com (Y. Xue).

0034-4257/$ – see front matter © 2012 Elsevier Inc. All rights reserved.
http://dx.doi.org/10.1016/j.rse.2012.10.009

2012), ALOMAR-Andenes, Abisko and Sodankyl stations (Rodríguez et al., 2007, 2011). Many research campaigns, such as ACE (Atmospheric Chemistry Experiment) (Bernath et al., 2005), ARCTAS (Arctic Research of the Composition of the Troposphere from Aircraft and Satellites) (Jacob et al., 2010), ARCPAC (Aerosol, Radiation, and Cloud Processes affecting Arctic Climate) (Brock et al., 2011), Chinese-Xuelong Arctic experiment (Lu & Bian, 2011), ASCOS (Arctic Summer Cloud Ocean Study) (http://www.ascos.se/, Chang et al., 2011), ASTAR (Arctic Study of Tropospheric Aerosols, clouds and Radiation) (http://www.pa.op.dlr.de/aerosol/astar2007/) CRAICC (http://www.atm.helsinki.fi/craicc/), CICCI (Cooperative Investigation of Climate Cryosphere Interaction) (http://niflheim.nilu.no/cicci) or ISDAC (Indirect and Semi-Direct Aerosol Campaign) (http://acrf-campaign.arm.gov/isdac/), have been conducted or are planned to be conducted in order to collect this information. In addition to these large international collaborative experiments, smaller campaigns such as Aerosol Arctic Campaign at ALOMAR (Cachorro, et al., 2003) provide very useful datasets. The experiments above mainly focus on interactions such as cloud-aerosol or aerosol-trace gas. Long term observation networks have been established which operate in the Arctic such as POLAR-AOD (Aerosols Optical Depth in Polar Regions: http://polaraod.isti.cnr.it:8080/Polar/) and part of AERONET (AErosol RObotic NETwork: http://aeronet.gsfc.nasa.gov/) (Holben et al., 1998), which provide long-term data sets for atmosphere component analysis and modelling validation.

However, ground-based observations are representative for a limited area (Mei et al., 2011). Information on long-range transport of particles to the Arctic is mainly obtained from model simulations and air mass trajectory analyses (Stohl, 2006). Satellite remote sensing would provide a complementary source of information. However, aerosol information such as the aerosol optical depth (AOD) is hard to retrieve at high latitudes such as the polar areas due to the high reflectance of snow and ice surfaces and additional problems associated with large solar zenith angles at these high latitudes. Therefore, aerosol remote sensing has hardly been used in the Arctic region (Istomina et al., 2011). Operational satellite aerosol products do not cover most of the Arctic region.

Snow covered surfaces are a great challenge for aerosol remote sensing because the surface contribution dominates the Top of Atmosphere (TOA) radiance measured by a satellite-based instrument. One of the crucial issues for the retrieval of aerosol properties from satellite-observed radiances is separating and explicitly describing the contributions from the reflection of solar radiation at the surface and backscattering by aerosol particles to the TOA radiance (Govaerts et al., 2010; Hsu et al., 2004; Martonchik et al., 2009). Over highly reflecting surfaces, the contribution of aerosols to the TOA radiation is very small as compared to the surface contribution.

Algorithms for aerosol retrieval over land have been developed for different sensors (see Kokhanovsky and de Leeuw (2009) and de Leeuw et al. (2011) for an overview). Examples are the European Space Agency (ESA) MEdium Resolution Imaging Spectrometer (MERIS) algorithm (Santer et al., 1999,) and Bremen AErosol Retrieval (BAER) for MERIS (von Hoyningen-Huene et al., 2003, 2011), the Along-Track Scanning Radiometer (ATSR-2) and Advanced ATRS (AATSR) dual view algorithm (ADV) (Curier et al., 2009; Kolmonen et al., 2012; Veefkind et al., 1998), the Swansea University AATSR algorithm (Grey et al., 2006), the Jet Propulsion Laboratory (JPL) algorithm for Multiangle Imaging Spectroradiometer (MISR) (Diner et al., 2005), the Dark Dense Vegetation (DDV) algorithm (Kaufman et al., 1997; Levy et al., 2007; Remer et al., 2006) and the DeepBlue algorithm (Hsu et al., 2004) for the Moderate Resolution Imaging Spectroradiometer (MODIS), the Centre National d'Etudes Spatiales (CNES) algorithm (Deuze et al., 2001) for POLarization and Directionality of the Earth's Reflectance instrument (POLDER) and optimal estimation for Meteosat Second Generation–Spinning Enhanced Visible and Infrared Imagers (MSG/SEVIRI) (Govaerts et al., 2010). All of these algorithms are suitable for certain ground surface conditions. However, there are no retrieval products over snow and ice surfaces and also highly reflective surfaces such as the Sahara desert pose a problem for some of the algorithms. For example, one major limitation of the MODIS Dense Dark Vegetation (DDV) approach is that no retrievals are performed when the surface reflectance at 2.1-μm is larger than 0.15, and the assumption of transparency in this channel does not apply (Hsu et al., 2004; Kaufman et al., 1997; Remer et al., 2005). Even though the relationship of visible to 2.12 μm surface reflectance is improved as a function of geometry, surface type (Gatebe et al., 2001; Remer et al., 2001) and scattering angle (Levy et al., 2007), this approach is still not effective for bright surfaces. Hsu et al. (2004) developed the deep blue approach to retrieve aerosol properties over surfaces such as arid, semi-arid and urban areas, where the surface reflectance in the blue spectral region is much darker than at longer wavelengths, with an estimated accuracy of 20–30%. However, this approach is also restricted to certain geometric limitations because some assumptions do not apply to large SZA. In the Arctic region, the surface albedo can exceed 0.85 in areas covered by snow. Besides the high reflectance of snow and ice, the strong BRDF effect of snow and ice is another problem and even a simple assumption for the BRDF can greatly improve aerosol retrievals versus the use of a Lambertian correction (Borde & Verdebout, 2003). However, the uncertainty in AOD retrieval over snow due to the BRDF effect is still far from being understood. Some measurements and parameterization methods have been used to study the BRDF of snow in regions such as Hokkaido, Japan (Aoki et al., 2000; Kokhanovsky et al., 2005), or the Antarctic considering effects of the macroscale surface roughness in polar snow (Hudson et al., 2006).

Istomina et al. tried to use the dual-view method at wavelengths in the visible (Istomina et al., 2009) and infrared (Istomina et al., 2011) spectral regions to retrieve AOD over Arctic regions using AATSR data. Kahn (2008) investigated the possibility of aerosol retrieval over snow using the Multi-angle Imaging SpectroRadiometer (MISR) (http://www.espo.nasa.gov/arctas/docs/presentations/Kahn_MISR_Overview.pdf), however, until now, no results have been published in the literature.

The longer atmospheric path length at large viewing angles, as encountered over the Arctic, enhances the contribution of aerosols to the signal received at TOA (Wagner et al., 2010), and thus enhances the possibility to retrieve aerosol properties. The AOD and surface reflectance, which are determined simultaneously based on prior knowledge, provide another way to obtain the AOD over a bright surface (Wang et al., 2012). Tang et al. (2005) proposed a method to accomplish aerosol retrieval over land by exploiting the synergy of the MODIS instruments on TERRA and AQUA. The method mainly uses the analytical solution provided by Xue and Cracknell (1995) and is suitable for non-absorbing aerosols. The method exploits synergetic measurements of different sensors which increases the information and can be used to solve the generally ill-posed or under-constrained Radiation Transfer Equations (RTE). For example, the same RTE can be used for different wavelengths of different observations while some parameters are wavelength-independent, that means more constraints can be obtained without increasing the unknowns. However, the use of different platforms may introduce additional uncertainties which need to be accounted for, such as accurate temporary and spatial co-registration of data from different platforms.

The use of prior knowledge, such as the surface characteristics, the aerosol physical, chemical and/or optical properties, the spatial distribution and temporal variation can be used to improve the retrieval accuracy. As mentioned above, a priori information on the surface characteristics can be used to improve the accuracy of AOD retrieval, especially over bright surfaces. In this paper, we assume that the ratio between surface reflectances at the same wavelength but from different observations can be determined using a snow BRDF model based on the Raman–Pinty–Verstraete model (RPV) (Maignan et al., 2004). As to the character of aerosol, historical datasets of aerosol properties were collected to serve as a basis for providing a reasonable first guess for use as an a priori in the retrieval.

Xue and Cracknell (1995) presented an operational bi-angle approach for retrieval of aerosol properties which does not consider absorption. This approach was applied over land surfaces by Tang et al. (2005) and Wang et al. (2012). In this paper we build on this work to derive the Aerosol Properties Retrieval over Snow (APRS) algorithm considering absorption using a two-stream approximation (Wang, personal communication, 2011). In APRS, the snow BRDF model is used to describe the surface properties. APRS is described in detail in Section 2. It is applied to data described in Section 3. In Section 4 the derived AOD is compared to AERONET (Holben et al., 1998) observations in the Arctic region. Conclusions are presented in Section 5.

2. Retrieval strategy

2.1. Radiative transfer model

The main concept of the most frequently used approximate radiative transfer equations consists of substituting the exact integrodifferential equation for radiant intensity by common differential equations for the upward and incident radiation fluxes (Kondratyev, 1969; Xue & Cracknell, 1995). The basic equation for the transfer of radiation in plane-parallel atmospheres can be decomposed into two differential equations: one for the upward radiant flux (denoted as $F^{(1)}(\tau)$), and one for the downward radiant flux (denoted as $F^{(2)}(\tau)$) (Kondratyev, 1969; Kuzetzov, 1942):

$$\frac{dF^{(1)}(\tau)}{d\tau} = -m^{(1)}(\tau)\left[k+\sigma\Gamma^{(1)}(\tau)\right]F^{(1)}(\tau) + m^{(2)}(\tau)\sigma\Gamma^{(2)}(\tau)F^{(2)}(\tau) \quad (1)$$

$$-\frac{dF^{(2)}(\tau)}{d\tau} = m^{(1)}(\tau)\sigma\Gamma^{(2)}(\tau)F^{(1)}(\tau) - m^{(2)}(\tau)\left[k+\sigma\Gamma^{(2)}(\tau)\right]F^{(2)}(\tau) \quad (2)$$

where

$$m^{(1)}(\tau) = \frac{\int_0^{2\pi} I^{(1)}(\tau,r')d\Omega}{\int_0^{2\pi} I^{(1)}(\tau,r')\cos\theta_0 d\Omega} \quad m^{(2)}(\tau) = \frac{\int_0^{2\pi} I^{(2)}(\tau,r')d\Omega}{\int_0^{2\pi} I^{(2)}(\tau,r')\cos\theta_0 d\Omega}$$

$$\Gamma^{(1)}(\tau) = \frac{\int_0^{2\pi} I^{(1)}(\tau,r')\beta^{(1)}(r')d\Omega}{\int_0^{2\pi} I^{(1)}(\tau,r')d\Omega}\Gamma^{(2)}(\tau) = \frac{\int_0^{2\pi} I^{(2)}(\tau,r')\beta^{(2)}(r')d\Omega}{\int_0^{2\pi} I^{(2)}(\tau,r')d\Omega}$$

$$\beta^{(1)}(r') = \frac{1}{4\pi}\int_0^{2\pi}\gamma^{(1)}(\tau,r',r)d\Omega \quad \beta^{(2)}(r') = \frac{1}{4\pi}\int_0^{2\pi}\gamma^{(2)}(\tau,r',r)d\Omega$$

$$I^{(1)}(\tau,r) = I(\tau,r) I^{(2)}(\tau,r) = I(\tau,-r)$$

$$\gamma^{(1)}(\tau,r',r) = \gamma(\tau,-r',r) \quad \gamma^{(2)}(\tau,r',r) = \gamma(\tau,r',-r)$$

r' stands for the direction of the incident radiation (μ_0,ϕ_0). $\mu_0 = \cos(\theta_0)$, θ_0 stands for the solar zenith angle, and ϕ_0 is the solar azimuth angle. r stands for the direction of the reflected radiation (μ,ϕ) $\mu = \cos(\theta)$, θ stands for the viewing zenith angle, and ϕ is the sensor azimuth angle. '−' indicates the opposite direction. Ω is the solid angle. k is the absorption coefficient, and σ is the scattering coefficient. τ is the atmospheric optical depth, which consists of two parts: the molecular scattering, also called Rayleigh scattering (τ_m) and the scattering by aerosol particles (τ_A), i.e. $\tau = \tau_A + \tau_m$. Here other gas effects rather than aerosol have been accounted for in the pre-processing. $I^{(1)}(\tau,r')$ and $I^{(2)}(\tau,r')$ are upward and downward radiant intensities respectively, and $\gamma(\tau,r',r)$ is the phase function that characterizes the scattered light intensity distribution in the direction (r',r). Under the assumption that $I(\tau,r')$ is angular independent, $\Gamma(\tau) = \beta(r')$.

With the following boundary conditions for the upward and downward fluxes at the top and the bottom of the atmosphere,

$$F^{(2)}(\tau = \tau_0) = E_0^{\lambda}\cos\theta_0, \quad (3)$$

$$F^{(1)}(\tau = 0) = R' F^{(2)}(\tau = 0), \quad (4)$$

where E_0^{λ} is the extraterrestrial solar irradiance, the relationship between the ground surface reflectance R and the TOA reflectance R' can be found:

$$R = \frac{(1-R'M_1)e^{\rho_1\tau} + (R'M_2-1)e^{\rho_2\tau}}{(R'M_2-1)M_1 e^{\rho_2\tau} + (1-R'M_1)M_2 e^{\rho_1\tau}} \quad (5)$$

where

$$M_1 = \frac{m^{(1)}(1-\omega) + m^{(1)}\omega\Gamma + \rho_1}{m^{(2)}\omega\Gamma}, M_2 = \frac{m^{(1)}(1-\omega) + m^{(1)}\omega\Gamma + \rho_2}{m^{(2)}\omega\Gamma}$$

$$\rho_1 = \frac{\left(m^{(2)}-m^{(1)}\right)(1-\omega+\omega\Gamma) + \sqrt{(m^{(1)}-m^{(2)})^2(1-\omega+\omega\Gamma)^2 + 4m^{(1)}m^{(2)}(1-\omega)(1-\omega+2\omega\Gamma)}}{2}$$

$$\rho_2 = \frac{\left(m^{(2)}-m^{(1)}\right)(1-\omega+\omega\Gamma) - \sqrt{(m^{(1)}-m^{(2)})^2(1-\omega+\omega\Gamma)^2 + 4m^{(1)}m^{(2)}(1-\omega)(1-\omega+2\omega\Gamma)}}{2}$$

$m^{(1)} = m^{(1)}(\tau) = 2$, $m^{(2)} = m^{(2)}(\tau) = \sec\theta$, $\Gamma = \Gamma(\tau)$, and ϖ is single scattering albedo. The problem here is how to estimate $\Gamma(\tau)$. The phase function $\gamma(\tau,r',r)$ is composed of two parts: the Rayleigh phase function $\gamma_m(\tau,r',r)$ and the aerosol phase function $\gamma_a(\tau,r',r)$ and $\gamma(\tau,r',r) = \frac{\tau_m}{\tau}\gamma_m(\tau,r',r) + \frac{\tau_a}{\tau}\gamma_a(\tau,r',r)$ (Wang, personal communication, 2011). The Rayleigh phase function is given by $\gamma_m(\tau,r',r) = \frac{3}{16}\left(1+\cos^2\psi\right)$, where ψ is the scattering angle. For the aerosol phase function we use results obtained from ground-based measurements during the Arctic haze event on 23, March, 2003, at Spitsbergen (78.923N, 11.923E) (Istomina et al., 2009) (see Fig. 1).

$$\begin{aligned}\Gamma &= \frac{1}{4\pi}\int_0^{2\pi}\gamma(\tau,r',r)d\Omega \\ &= \frac{1}{4\pi}\int_0^{2\pi}\int_0^{\frac{\pi}{2}}\left[\frac{3}{4}\left(1+\cos^2\vartheta\right)\tau^m/\tau + \gamma_a(\psi)\tau^a/\tau\right]\sin\psi d\psi d\varphi \\ &= \frac{\tau^m}{2\tau} + \frac{\tau^a}{2\tau}\int_0^{\frac{\pi}{2}}\gamma_a(\psi)\sin\psi d\psi\end{aligned} \quad (6)$$

Here $\int_0^{\frac{\pi}{2}}\gamma_a(\psi)\sin\psi d\psi \approx \sum_{l=0}^{n}\frac{\gamma_a(\psi_i)\sin\psi_l + \gamma_a(\psi_{l-1})\sin\psi_{l-1}}{2}\times(\psi_l-\psi_{l-1})$ and n stands for the number of observations of the scattering angle. If the aerosol phase function is unknown, the H–G analytical phase function can be used (Henyey & Greenstein, 1941). Then $\gamma_a(\psi) = \frac{1-g^2}{[1+g^2-2g\cos(r',r)]^{3/2}}$ and we can finally obtain $\Gamma = \frac{\tau_m}{2\tau} + \frac{\tau_a(1-g)}{2g\tau}\left[\frac{1+g}{(1+g^2)^{1/2}}-1\right]$, here g is Asymmetry factor.

2.2. Sensitivity study

In this section a sensitivity analysis (SA) is presented to determine how different sources of uncertainty influence the uncertainty in the retrieval result (Saltelli et al., 2008), in particular the sensitivity of

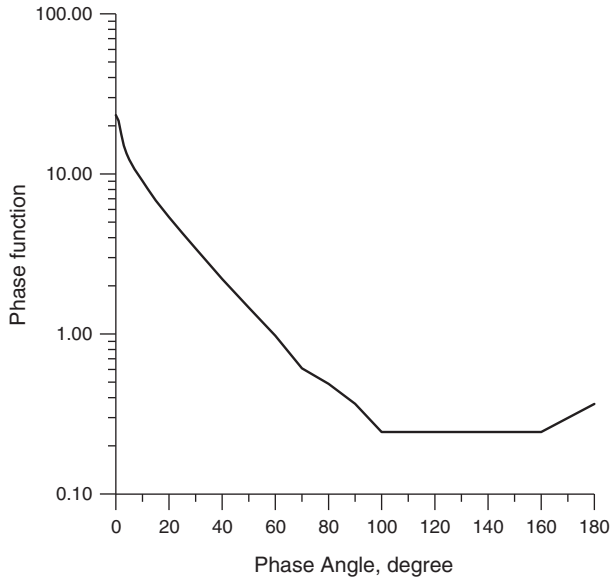

Fig. 1. Phase function of Arctic haze aerosol used for retrieval. Adopted from Istomina et al. (2009).

Eq. (5). In order to simplify the analysis procedure, a case that is considered without absorption for Eq. (5) was displayed as follows:

If we consider the atmosphere without absorption, Eq. (5) can be simplified to:

$$R = \frac{(bR'-a) + a(1-R')e^{(a-b)\varepsilon\tau}}{(bR'-a) + b(1-R')e^{(a-b)\varepsilon\tau}} \tag{7}$$

where $a = 1/\mu_0$, $b = 2$, ε is the backscattering coefficient, typically 0.1, which is the same as used in Xue and Cracknell (1995).

We can rewrite Eq. (7) as follows:

$$\tau = \frac{1}{\varepsilon(a-b)} \ln\left\{\frac{(R'b-a)(1-R)}{(Rb-a)(1-R')}\right\}. \tag{8}$$

Eq. (8) is used to investigate the error in determining AOD related to uncertainties in the TOA reflectance R'. The relative uncertainty can be evaluated from Eq. (8) as:

$$\frac{\Delta\tau}{\Delta R'} = \frac{1}{\varepsilon}\frac{1}{(a-R'b)(1-R')}. \tag{9}$$

The accuracy of the AOD depends mostly on the SZA and the value of the TOA reflectance.

In the sensitivity study, the standard Arctic aerosol type from the Optical Properties of Aerosols and Clouds (OPAC) data base (Hess et al., 1998) was used. The particle size distribution is described by a log-normal distribution:

$$f(r) = \frac{1}{\sqrt{2\pi}\sigma_0 r_0} \exp\left[-\frac{\ln^2\left(\frac{r}{r_0}\right)}{2{\sigma_0}^2}\right], \tag{10}$$

where r is the radius of a spherical homogeneous particle and $\int_0^\infty f(r)dr = 1$. r_0 is the average geometrical radius and σ_0 is the geometric standard deviation. Aerosol phase functions and the single scattering albedo for spherical particles at different wavelengths have been calculated using OPAC.

In general, the TOA reflectance over a dark surface increases with the aerosol load, while over a bright surface an increasing aerosol load would cause darkening of the scene at wavelengths in the visible spectral region. The critical reflectance divides the positive effect and negative effect of aerosol: for a certain value of the critical reflectance the darkening is insensitive to AOD. This is illustrated in Fig. 2, where the AOD is plotted as a function of the TOA reflectance for SZA of 30° and 65°. The curves shown in Fig. 2 were calculated for surface reflectances varying from 0 to 1.0. The TOA critical reflectance is around 0.23 for SZA = 30° and around 0.35 for SZA = 65°. Fig. 2 also shows that Eq. (5) applies only to AOD values smaller than 5.0, especially for large SZAs. This is because Eq. (5) was derived using a boundary condition for the surface properties, which implies that the surface needs to be visible. However, if the AOD is very large, no surface information can be obtained and Eq (5) cannot be applied. It is obvious that the AOD sensitivity (the gradients in Fig. 2) depends

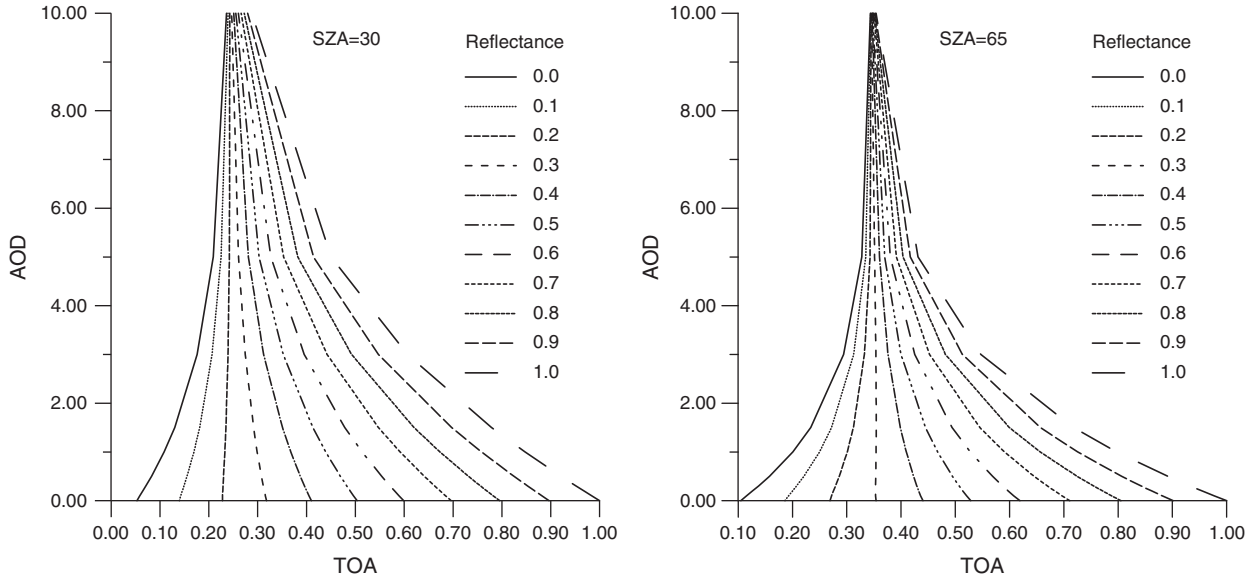

Fig. 2. Sensitivity analysis for Eq. (5): the AOD is plotted as function of the TOA reflectance, for a range of surface reflectances (see legend) and for 2 solar zenith angles.

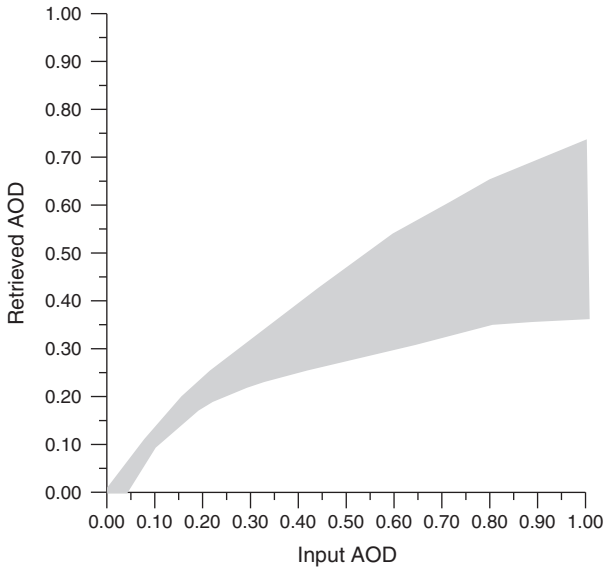

Fig. 3. The dependence of the retrieved AOD on the input AOD for the RT simulated TOA reflectance. For this sensitivity study, the input reflectance was varied by +/− 2% with certain input AOD, which resulted in deviations in the retrieved AOD: for an increase of the input reflectance with 2% the lowest values were retrieved (lower border of the colour filled area), for a decrease of the input reflectance with 2% the higher AOD values were retrieved. In these simulations the single scattering albedo was set equal to 0.9.

strongly on the surface properties and it decreases with increasing reflectance smaller than the critical reflectance, while for reflectances larger than the critical reflectance the sensitivity increases. That means that Eq. (5) can be applied over snow (TOA reflectance between 0.6 and 1.0) as well as for dark surfaces with reflectances smaller than 0.6. The reflectance of snow may be larger than 0.6 but the satellite sensor "sees" the signal averaged on a certain area (the pixel) and the pixel reflectance is not necessarily larger than 0.6 (i.e. in the presence of trees). The reflectance for melting snow is around 0.6 and for fresh snow it is around 0.9 or even larger in the Arctic. The sensitivity study shows that the contributions from aerosol and surface reflectance to the TOA reflectance can be separated at large SZAs. It is important to note that these effects are only valid when the absorption is small. If we assume that the SZA = 65°, the snow reflectance is 0.85, with a TOA reflectance uncertainty of 5%, we can calculate that the corresponding propagated uncertainty for AOD retrieval error is around 0.02 for AOD smaller than 1.0. The analysis above shows that Eq. (5) provides a method for AOD retrieval over bright surfaces at large solar zenith angles in the Arctic region.

2.3. Inverse problem

The wavelength dependence of atmospheric scattering, composed of molecular (Rayleigh) scattering and scattering by aerosol particles can be expressed as follows (Ångström, 1929):

$$\tau_a = \beta\lambda^{-\alpha} \tag{11}$$

where β is Ångström's turbidity coefficient, α is the Ångström coefficient, and λ is the wavelength. Linke (1956) provided an approximation for Rayleigh scattering:

$$\tau_m = -0.00897\lambda^{-4.09} \tag{12}$$

Flowerdew and Haigh (1995) proposed that the surface reflectance can be approximated by a part which describes the variation with the wavelength and a part which describes the variation with the geometry. In other words, the ratio of observations at different viewing angles is independent of wavelength. With this assumption, the ratio of the surface reflectances subsequently observed by TERRA/MODIS and AQUA/MODIS can be expressed as:

$$K_{\lambda_i} = \frac{R_{\mathrm{Terra},\lambda_i}}{R_{\mathrm{Aqua},\lambda_i}}, \tag{13}$$

where $R_{\mathrm{Terra},\lambda_i}$ stands for the surface reflectance observed by MODIS during the TERRA overpass of the study area, and $R_{\mathrm{Aqua},\lambda_i}$ is the surface reflectance observed by MODIS on AQUA. Here λ_i stands for different wavelengths of the MODIS sensor. Eq. (13) was used in previous studies by assuming that reflectance ratio can be obtained at a wavelength of 2.1 μm using the assumption that the aerosol contributions to the TOA reflectances at this wavelength are negligible (Tang et al., 2005; Wang et al., 2012). However, this method was not applicable over the Arctic because the ratio of the reflectances at different wavelengths varies significantly at large SZA, especially for surfaces with a strong BRDF effect. This has been further evaluated by calculating the ratio of the reflectances at 0.55 μm and 2.1 μm provided by the MODIS surface reflectance product (MOD/MYD09) over west Greenland, which is the study area in this paper. The statistic analysis shows that the difference between ratios of the reflectances at these two wavelengths is larger than 0.2 for more than 70% of the points, which will bring about uncertainties of at least 0.1 when using Eq. (5) (see Fig. 2). To solve this problem, we use a snow BRDF model to estimate the reflectance ratio at the same wavelengths as the satellite observations. To this end, we use the snow BRDF model by Kokhanovsky et al. (2005), which is a good parameterization of the snow spectral reflection function R_s (μ,μ_0,ϕ,ϕ_0):

$$R_s(\mu,\mu_0,\phi,\phi_0) = R_0(\mu,\mu_0,\phi,\phi_0)A^{f(\mu,\mu_0,\phi,\phi_0)} \tag{14}$$

where

$$A = \exp\left\{\frac{-4s}{\sqrt{3}}\right\}, s = \sqrt{\frac{1-\varpi}{1-g\varpi}}, f = \frac{u(\mu)u(\mu_0)}{R_0(\mu,\mu_0,\phi)}, u(\mu) = \frac{3}{7}(1+2\mu)$$

$$R_0(\mu,\mu_0,\phi,\phi_0) = \frac{c + d(\mu+\mu_0) + e\mu\mu_0 + p(\psi)}{4(\mu+\mu_0)}.$$

Here R_0 (μ,μ_0,ϕ,ϕ_0) is the reflection function of non-absorbing snow, g is the asymmetry factor, ϖ is the single scattering albedo, $c = 1.247$, $d = 1.186$, $e = 5.157$, ψ is the scattering angle, and $p(\psi) = 11.1\exp(-0.087\psi) + 1.1\exp(-0.014\psi)$.

Table 1
Six selected AERONET stations in the Arctic region and their location (latitude, longitude and altitude) selected for our aerosol retrieval validation.

Number	Name	Longitude (° East)	Latitude (° North)	Altitude(m)
1	Andenes	16.008611	69.278333	379
2	Barrow	−156.665	71.3122	0
3	Ittoqqortoormiit	−21.9512	70.4848	68
4	OPAL	−85.939167	79.990278	0
5	Thule	−68.769001	76.516102	225
6	PEARL	−86.416944	80.053611	615

Painter and Dozier (2004) found that the snow grain size has little influence on snow BRDF effect at short wavelengths. At these wavelengths the influence of grain size and shape is limited due to low absorption and the large number of scattering events. In view of the high solar zenith angle in the Arctic, an air mass correction is also needed. Here we use the air mass factor given by Kasten and Young (1989). Topography is another factor which may affect the retrieval accuracy. Lacking a very high accuracy dataset, this factor was not considered in the present study. Fröhlich and Shaw (1980) pointed out that neglecting topography in Eq. (12) may cause an error of $\pm 0.7\%$ in the Rayleigh optical depth. On the other hand, the snow BRDF model used in the paper was developed based on the assumption of a plane-

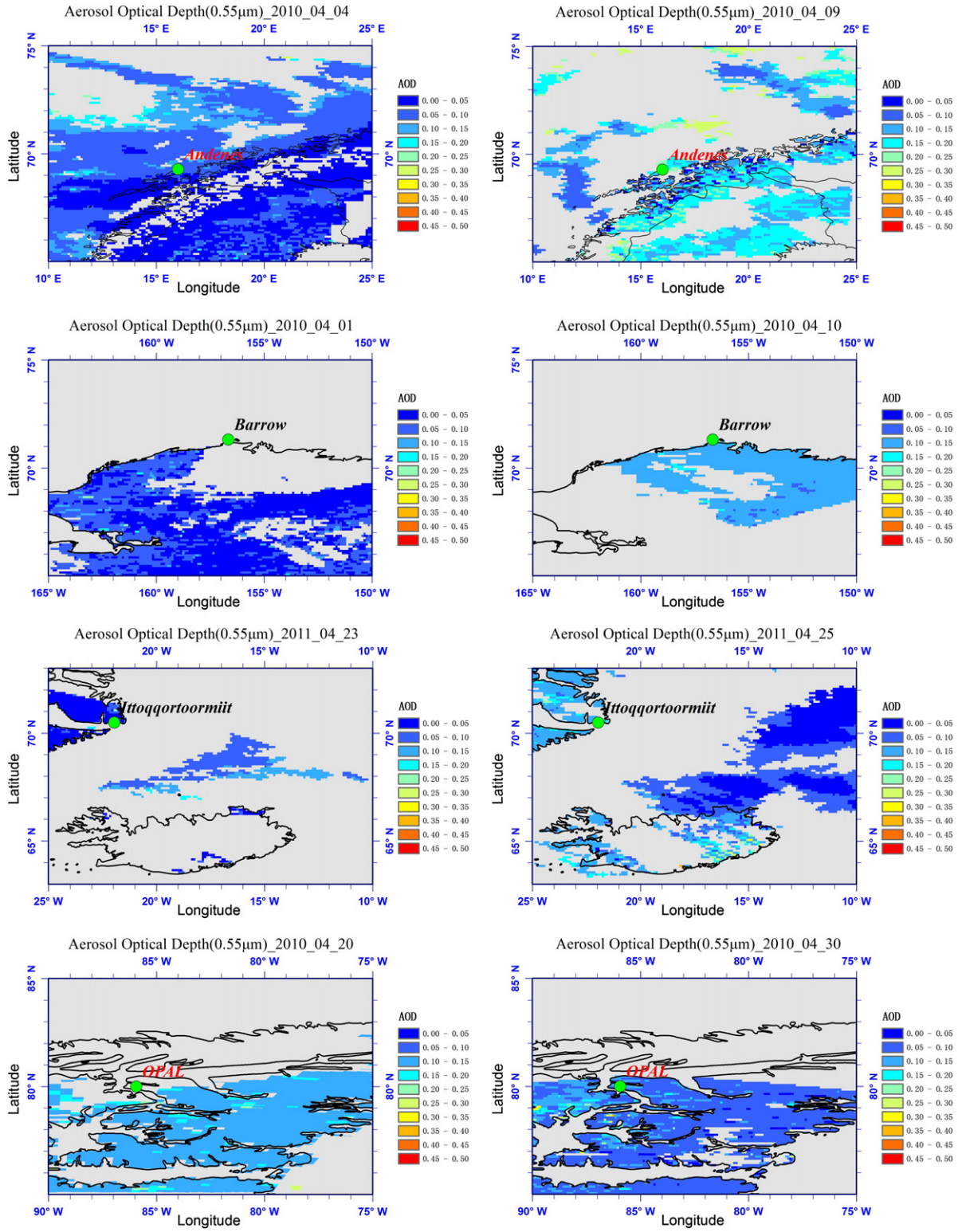

Fig. 4. Aerosol optical depth derived at 550 nm of the TERRA overpass with 10 km resolution on two different days for each AERONET site, using the APRS method described in Section 2 (AOD values over ocean were provided by NASA MODIS DDV product).

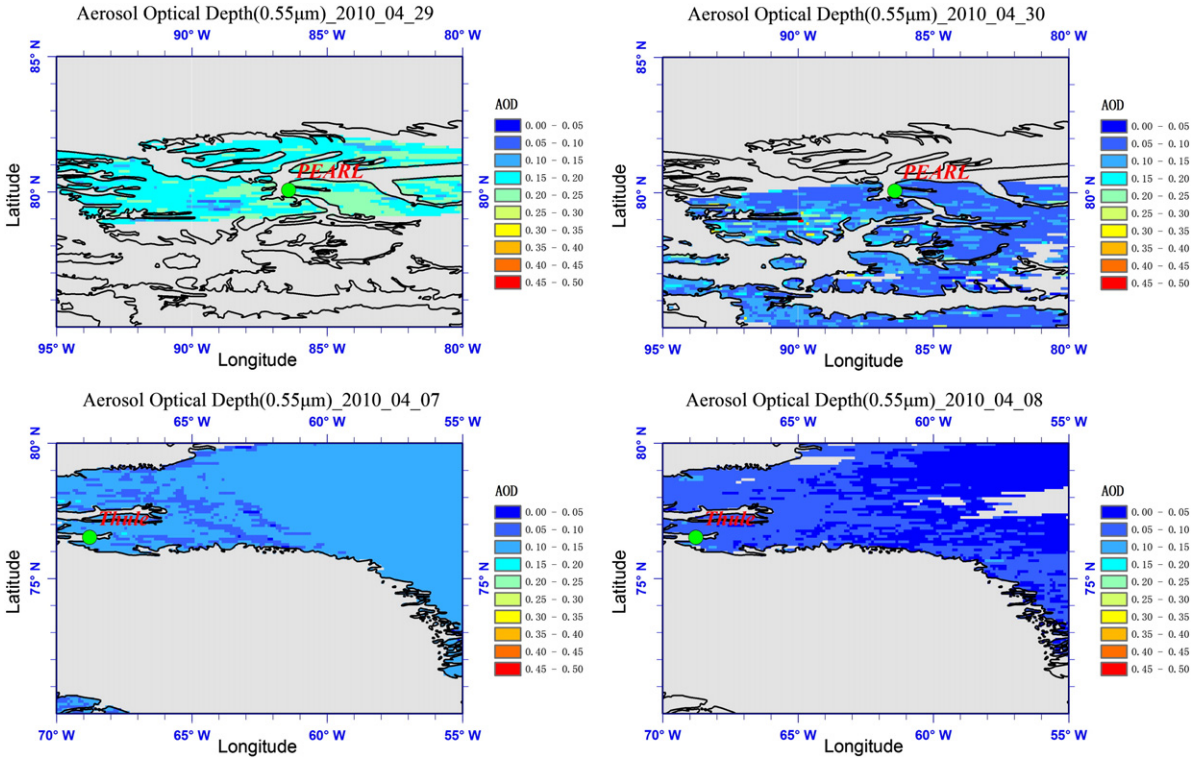

Fig. 4 (*continued*).

parallel layer (Kokhanovsky et al., 2005), topography can also affect the snow BRDF estimation and cause an uncertainty in the AOD retrieval.

The time interval between the Terra and Aqua over-passes is around 100 min (Key et al., 2003). Over the Arctic region, the time difference is actually smaller, because of the wide swath of MODIS, and it is easy to find regions observed by TERRA/MODIS and AQUA/MODIS within a very short time (between 20 and 30 min for data used in this manuscript). We assumed that between observations within such a short time interval the aerosol types and properties α do not change, but β (Ångström's turbidity coefficient) may be different during the TERRA (denoted as $\beta 1$) overpass from that during the AQUA (denoted as $\beta 2$) overpass, and the AOD was retrieved using the three visible bands (0.47 μm, 0.55 μm and 0.66 μm) of TERRA/MODIS and AQUA/MODIS:

$$\sum_{i=1}^{j}\left(\frac{R^{\mathrm{RTE}}{}_{Terra,\lambda_i}}{R^{\mathrm{RTE}}{}_{Aqua,\lambda_i}}-\frac{R^{\mathrm{BRDF}}{}_{Terra,\lambda_i}}{R^{\mathrm{BRDF}}{}_{Aqua,\lambda_i}}\right)^2<\chi. \tag{15}$$

In Eq. (15), j indicates the three different wavelengths, R^{RTE} and R^{BEDF} stand for reflectance calculated using the RTE and the reflectance calculated using the BRDF model. In Eq. (15), there are 3 unknowns (α, $\beta 1$ and $\beta 2$) with 3 non-linear equations (one for each wavelength), χ is the condition to stop the iteration of Eq. (15), $\chi = 10\mathrm{E}-5$ in the Interactive Data Language (IDL) programme. Then the Levenberg–Marquardt algorithm (Levenberg, 1944) was used to obtain the solution of Eq. (15). After obtaining the solution for α, $\beta 1$ and $\beta 2$ using cost function Eq. (15), AOD was calculated using Eq. (11) for three wavelengths (0.47, 0.55 and 0.66 μm) for both TERRA (TERRA AOD, expressed as $\beta_1\lambda^{-\alpha}$) and AQUA (AQUA AOD, expressed as $\beta_2\lambda^{-\alpha}$).

The retrieval requires prior knowledge as an initial guess for solving the non-linear Eq. (15). To this end, historical datasets (here we use the average value of one week before retrieval), including MODIS standard AOD products and ground-based measurements, were collected and used to calculate the Ångström coefficient. This value is interpolated assuming that the correlation between AOD over different pixels

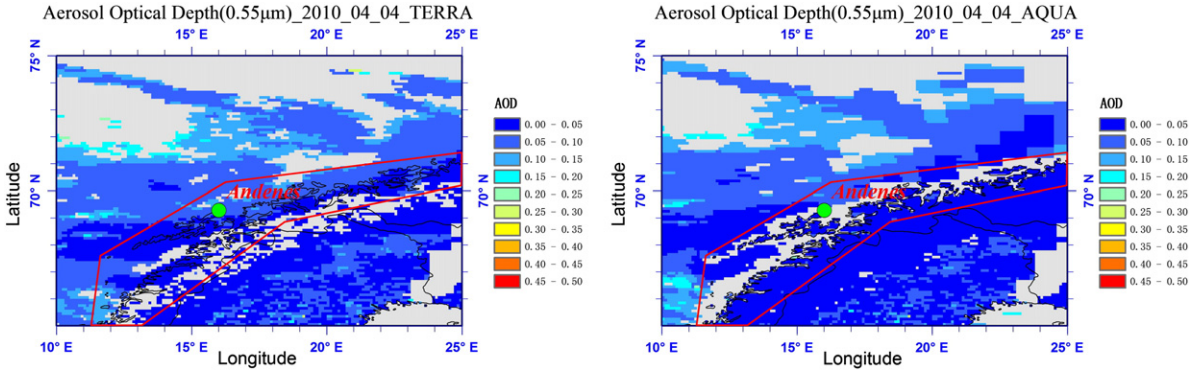

Fig. 5. Comparison of AOD derived at 550 nm from TERRA/MODIS and AQUA/MODIS with 10 km resolution on 4 April 2010. The red frame indicates the agreement between APRS result and MODIS DDV product.

decreases with increasing distance. For Arctic haze, Heintzenberg et al. (2003) suggested that $\alpha = 1.8$ while other researchers suggest that α is equal to or greater than 1.5 (Quinn et al., 2007). Obviously α varies between different haze events, but we use these values only as a reasonable first guess. If there is no historical dataset for the study area, we use as initial values AOD = 0.1 and $\alpha = 1.5$.

Fig. 3 shows the sensitivity of the retrieved AOD to the uncertainty of the TOA reflectance. The results show that an uncertainty of ±2% in the TOA reflectance the retrieval error has a value of approximately 0.04 for AOD smaller than 0.3,while for higher AOD the error increases substantially with increasing AOD. Fig. 3 also demonstrates that the retrieved AOD can be substantially underestimated for large AOD. However, such large AOD values are not common over the Arctic.

Due to the similarity of optical properties of snow and clouds, especially for ice clouds, in the visible band, cloud adjacency effects may cause a large error in the AOD retrieval. The ratio of the two observations (nadir and forward) can vary a lot because a cloud edge may observe in one viewing direction but not in the other one. If we assume that the cloud contributes 2% of TOA reflectance, the uncertainty in the derived AOD is about 10% when AOD = 0.2 (Fig. 3). Another effect, connected with clouds is cloud shadows (von Hoyningen-Huene et al., 2011), which may also cause bias of AOD. If we tried to remove the cloud effect manually, more reasonable AOD can be obtained. For instance, AOD reduced from 0.204 to 0.183 on site Ittoqqortoormiit on 25 April 2011.

3. Data

The datasets used in this study include satellite data and ground-based data. The satellite data include MODIS Level 1B data for AOD retrieval and Level 2 data, such as aerosol and cloud classification products, which were used for prior knowledge. MODIS Level 1B data is available through the LAADS website (http://modis.gsfc.nasa.gov/data/). MODIS data was resized to 10×10 km^2 in order to make it comparable to MODIS standard AOD products. Terra's orbit around the Earth is timed such that it passes from north to south across the equator in the morning, while Aqua passes south to north over the equator in the afternoon. The MODIS cloud classification product was used as a cloud mask for the current APRS Arctic region AOD retrieval.

Ground-based data was AERONET sun photometer data (Holben et al., 1998). AERONET provides globally distributed observations of spectral AOD at three data quality levels: Level 1.0 (unscreened), Level 1.5 (cloud-screened), and Level 2.0 (cloud-screened and quality-assured). Data from six AERONET sites at high latitudes (latitude greater than 65°) in the regions of interest during April 2010 (April 2011 for Ittoqqortoormiit because there were no AERONET data during April 2010) were collected as prior data for AOD retrieval and to see the Arctic haze phenomenon. Table 1 shows the information regarding latitude, longitude and elevation of the selected AERONET sites.

4. Results and validation

APRS was used to retrieve the AOD over land for selected regions in the Arctic using MODIS data for April 2010 (April 2011, for Ittoqqortoormiit). MODIS AODs over ocean were obtained from the NASA MODIS standard aerosol product. Examples of the spatial distribution of the AOD retrieved by APRS at a wavelength of 0.55 μm are shown in Fig. 4, for six different areas covering the AERONET sites. The results show that the AOD over all regions is quite low with values varying between 0.05 and 0.20 with some variability for most cases. For scenes where we have both AOD over land from APRS and over ocean from the NASA MODIS standard product (e.g. Andenes, Ittoqqortoormiit) we see a rather smooth transition from land to ocean which lends credibility to the APRS product. The AOD distribution in the scene covering Andenes shows some variation which may be due to the complex topography with its distribution of land masses and oceans. For OPAL and Thule, which are at the highest latitudes, the "background value" is less than 0.05. During Arctic haze events higher AOD values are observed, e.g. 0.18 (OPAL on 28 April 2010), or 0.4 (Thule on 9 April 2010).

As mentioned above, by using both MODIS/TERRA and MODIS/AQUA data, we can retrieve AODs at two overpass times. A comparison of the APRS MODIS Terra and AQUA retrievals using data for 4 April 2010, around Andenes is presented in Fig. 5. The AOD distributions retrieved from the TERRA and AQUA data are very similar. Fig. 5 also shows the rather smooth transition of the AOD over the ocean (obtained as the MODIS DDV product) and over the adjacent snow-covered surface obtained with APRS. The two independent methods over very different surfaces show similar results.

For the comparison of the APRS results with AERONET data we followed the methodology described in Ichoku et al. (2002). The wavelengths of MODIS (0.55 μm) and AERONET (0.5 μm) are slightly different, therefore the AERONET observations were converted to 0.55 μm by a quadratic polynomial fit of the natural logarithm of the AERONET AODs at different wavelengths to the wavelength (fitting error of about 0.01–0.02) (Eck et al., 1999) to provide the 0.55 μm AOD at the AERONET sites for comparison with the satellite-retrieved AODs. Wavelengths of 0.44, 0.675 and 0.87 μm were selected for fitting. Because the retrieved AOD resolution is 10×10 km^2, each collocated AERONET site (Table 1) was identified in each MODIS aerosol image using its latitude and longitude. On the temporary scale, the average values during a 1-hour period centred on the MODIS overpass time were extracted (Ichoku, et al., 2002).

Seventy matches were found for the AERONET and APRS data retrieved from Terra/MODIS measurements. We also use the MODIS cloud product to distinguish cloud from snow/ice. Fig. 6 shows the relationship between the APRS-retrieved AOD and AERONET AOD at 550 nm at different Arctic stations. The fit parameters obtained using a standard least-squares regression method show $R^2 = 0.664$ (i.e. correlation of about 0.8) and Root-Mean-Square-Error (RMSE) 0.079 with a bias of 0.049 and a slope of 0.764. If we consider the uncertainty of ground-based measurement and use the York regression method (Cantrell, 2008), we may obtain a slope closer to 1 and a smaller bias (Fig. 6). The results in Fig. 6, showing the favourable agreement between APRS and AERONET values, indicate the suitability of the APRS method to retrieve AOD over the Arctic with highly reflecting snow/ice surfaces and large SZAs. Imperfect cloud screening, discussed below, may be the main reason for the deviations of slope and bias.

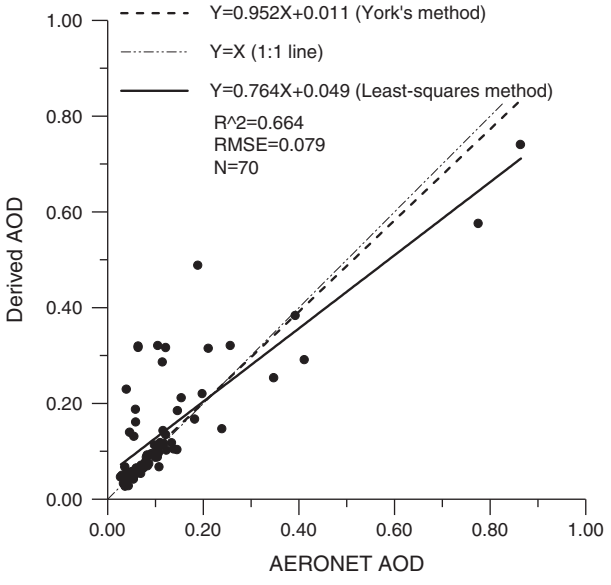

Fig. 6. Relationship between AODs derived from MODIS data with 10 km × 10 km resolution and AODs from AERONET observation at 550 nm during April 2010 (for site Ittoqqortoormiit April 2011) by the APRS method at six Arctic stations. Here, RMSE means root-mean-square error and N is total number of matched cases.

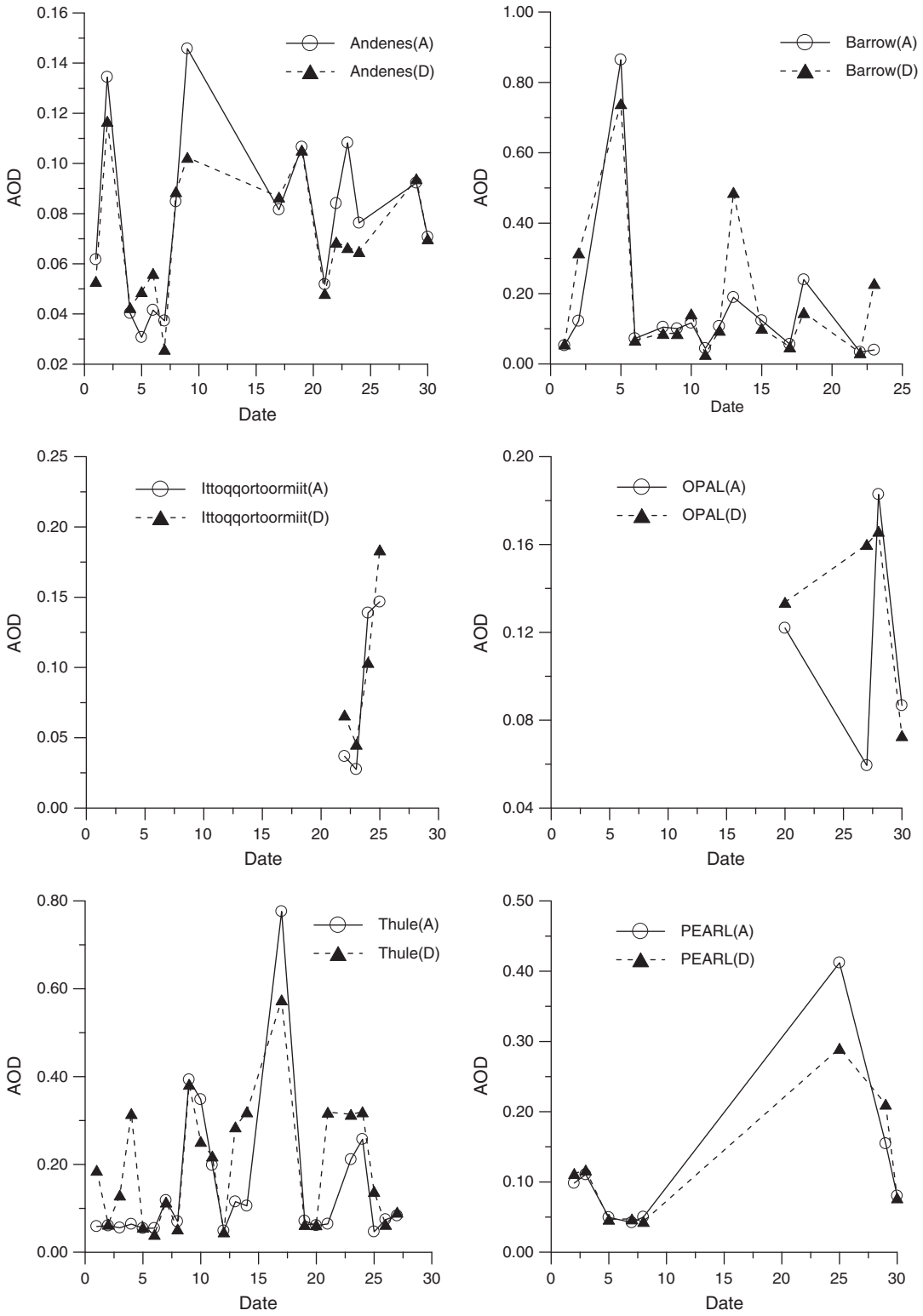

Fig. 7. Time series of AODs during study period at different AERONET stations: Andenes; Barrow; Ittoqqortoormiit; OPAL; Thule and PEARL (A stands for AERONET, and D stands for APRS-retrieved).

A comparison of time series of the APRS-retrieved and AERONET AOD values for each station is shown in Fig. 7. Retrieval and AERONET AOD values trace each other well for most cases, except for 23 April 2010 over Andenes, 13 and 23 April 2010 over Barrow, 27 April 2010 over OPAL, 1,4, 13, 14, 21 and 25 April 2010 over Thule when extremely high retrieval AODs were found. This is ascribed to the effect of cloud edges as identified by the cloud product. All time series results show that the AOD over the Arctic is very low but with quite some variability.

5. Conclusions

The APRS method has been developed to retrieve aerosol properties over the Arctic, i.e. over highly reflective surfaces at large solar

zenith angles. The results compare favourably with independent AOD measurements both as regards the value of the AOD and the temporal trends. The APRS method has a relatively high level of accuracy (the correlation between retrieval AOD and ground-based measurement is greater than 0.8 with RMSE = 0.079).

The APRS method uses synergetic measurements of two satellites. It relies on the high radiometric accuracy and accurate co-registration of two images which were measured at different times. A plane-parallel radiative transfer model is used, limiting the applicability to data with SZA smaller than 75°. The snow BRDF model provided by Kokhanovsky et al. (2005) is a good approximation for pure and clear snow, which need to be improved in the future work because the Arctic surface is mixture of snow and ice for spring time. A linear mixture model between snow and ice may improve the retrieval accuracy. The effects of macro-scale surface roughness (Hudson et al., 2006) over the Arctic region may be another problem for snow BRDF ratio estimation.

APRS may overestimate the AOD, the most important reason for which is cloud contamination. MODIS standard snow and cloud products have been used to identify the occurrence of snow and clouds, but cloud edges remain a large problem. Only one aerosol type was used and particles were assumed to be spherical. This may be a cause of error in the estimation of aerosol properties, especially for the phase function. For a real case, the phase function is much smoother with scattering angle larger than 120°, without significant forward backscattering because of the non-spherical properties, especially for large SZA.

Further work will be conducted to include various BRDF models in order to get a more appropriate description of the surface properties in the retrieval procedure. A digital elevation model to account for the Rayleigh scattering and correction for air mass with large SZA will also be taken into account. As to the aerosol type, ground-based measurements (such as AERONET) will be used to provide more reliable aerosol properties such as phase function, or single scattering albedo.

Acknowledgements

This work was partly supported by the Major International Cooperation and Exchange Project of National Natural Science Foundation of China (grant no. 41120114001) and the Ministry of Science and Technology (MOST) of China under grant nos. 2010CB950802 and 2010CB950803. L.L. Mei would like to thank the Director Prize from the Institute of Remote Sensing Applications of Chinese Academy of Sciences. Thanks for the valuable discussion from Dr. Wang from Institute of Remote Sensing Applications, Chinese Academy of Sciences. The contribution of Gerrit de Leeuw is supported by CRAICC (Cryosphere–atmosphere interactions in a changing Arctic climate), which is part of the Top-level Research Initiative (TRI) of the joint Nordic research and innovation initiative. MODIS data were available through NASA MODIS LAADS. Many thanks are due to the PI investigators with the AERONET sites used in this paper.

Appendix A. List of symbols

Standard alphabetical symbol

Symbol	Description
E_0^{λ}	Extraterrestrial solar irradiance at wavelength λ
$F^{(1)}(\tau)$	Upward radiant flux at AOD equal to τ
$F^{(2)}(\tau)$	Downward radiant flux at AOD equal to τ
g	Asymmetry factor
i	Channel number of MODIS
$I^{(1)}(\tau,r')$	Upward radiant intensity at direction r' with AOD equal to τ
$I^{(2)}(\tau,r')$	Downward radiant intensity at direction r' with AOD equal to τ
J	Total MODIS channels used in the paper, here j = 3
K	Absorption coefficient
K_{λ_i}	Ratio between surface reflectances obtained from TERRA/MODIS and AQUA/MODIS at wavelength λ_i
N	Number of observations of the scattering angle
r'	Direction of the incident radiation, including solar zenith angle and solar azimuth angle
r	Direction of the reflected radiation, including viewing zenith angle and viewing azimuth angle
r_0	Average geometrical radius
R	Ground surface reflectance
$R_s(\mu,\mu_0,\phi,\phi_0)$	Snow spectral reflection function at certain geometry condition
R0 (μ,μ_0,ϕ,ϕ_0)	Reflection function of non-absorbing snow at certain geometry condition
R_{Terra,λ_i}	Surface reflectance observed by MODIS during the TERRA overpass of the study area
$R^{RTE}_{Terra,\lambda_i}$	Reflectance calculated using the RTE (Eq. (5)) for TERRA at wavelength λ_i
$R^{BRDF}_{Terra,\lambda_i}$	Reflectance calculated using the BRDF model (Eq. (14)) for TERRA observation at wavelength λ_i
R_{Aqua,λ_i}	Surface reflectance observed by MODIS/AQUA
R^{RTE}_{Aqua,λ_i}	Reflectance calculated using the RTE(Eq. (5)) for AQUA at wavelength λ_i
$R^{BRDF}_{Aqua,\lambda_i}$	Reflectance calculated using the BRDF model (Eq. (14)) for AQUA observation at wavelength λ_i
R'	TOA reflectance

Standard Greek symbols

Symbol	Description
α	Wavelength exponent in angstrom's turbidity formula
β	Angstrom's turbidity coefficient
$\beta 1$	Ångström's turbidity coefficient during TERRA overpass
$\beta 2$	Ångström's turbidity coefficient during AQUA overpass
$\gamma(\tau,r',r)$	Phase function that characterizes the scattered light intensity distribution in the direction (r',r)
$\gamma(\tau,r',r)$	Phase function that characterizes the scattered light intensity distribution in the direction $(-r',r)$,here $-r'$ stands for the opposite direction of r'
$\gamma(\tau,r',r)$	Phase function that characterizes the scattered light intensity distribution in the direction $(r',-r)$,here $-r$ stands for the opposite direction of $-r$
$\gamma_m(\tau,r',r)$	Rayleigh phase function
$\gamma_a(\tau,r',r)$	Aerosol phase function
ε	Backscattering coefficient, typically 0.1
θ	Viewing zenith angle
θ_0	Solar zenith angle
λ	Wavelength (μm)
λ_i	Different wavelengths of the MODIS sensor (μm)
μ	Cosine of view zenith angle
μ_0	Cosine of solar zenith angle
σ	Scattering coefficient
σ_0	Geometric standard deviation
τ	Atmospheric optical depth
τ_0	Total atmospheric optical depth for the whole atmosphere layer
τ_m	Rayleigh optical depth
τ_a	Aerosol optical depth
ϕ	Sensor azimuth angle
ϕ_0	Solar azimuth angle
χ	Condition to stop the iteration of Eq. (15)
ψ	Scattering angle
Ω	Solid angle
ϖ	Single scattering albedo

References

Ackerman, T. P., Stemback, J. N., & Valero, F. P. J. (1986). The importance of Arctic haze for the energy budget of the Arctic. *Arctic Air Pollution* (pp. 151–158). Cambridge: Cambridge University Press.

Ångström, A. (1929). On the atmospheric transmission of sun radiation and on dust in the air. *Geografiska Annaler, 11*, 156–169.

Aoki, T., Aoki, T., Fukabori, M., Hachikubo, A., Tachibana, Y., & Nishio, F. (2000). Effects of snow physical parameters on spectral albedo and bidirectional reflectance of snow

surface. *Journal of Geopysical Research*, *105*(D8), 10219–10236. http://dx.doi.org/10.1029/1999JD901122.
Bernath, P. F., McElroy, C. T., Abrams, M. C., Boone, C. D., Butler, M., Camy-Peyret, C., et al. (2005). Atmospheric Chemistry Experiment (ACE): Mission overview. *Geophysical Research Letters*, *32*, L15S01. http://dx.doi.org/10.1029/2005GL022386.
Borde, R., & Verdebout, J. (2003). Remote sensing of aerosol optical thickness over various sites using SeaWiFS or VEGETATION and ground measurement. *Remote Sensing of Environment*, *86*, 42–51.
Brock, C. A., Cozic, J., Bahreini, R., Froyd, K. D., Middlebrook, A. M., McComiskey, A., et al. (2011). Characteristics, sources, and transport of aerosols measured in spring 2008 during the aerosol, radiation, and cloud processes affecting Arctic Climate (ARCPAC) Project. *Atmospheric Chemistry and Physics*, *11*, 2423–2453.
Cachorro, V. E., De Frutos, A. M., Vergaz, R., & Mar Sorribas, M. (2003). Aerosol Arctic Campaign at ALOMAR (69N, 16E, Norway) in June–July 2002, 2003. *Proceedings of 2003 IEEE International Geoscience and Remote Sensing Symposium held in Toulouse, France*.
Cantrell, C. A. (2008). 2008, technical note: Review of methods for linear least-squares fitting of data and application to atmospheric chemistry problems. *Atmosphere Chemistry and Physics*, *8*, 5477–5487.
Chang, R. Y. -W., Leck, C., Graus, M., Müller, M., Paatero, J., Burkhart, J. F., et al. (2011). Aerosol composition and sources in the central Arctic Ocean during ASCOS. *Atmospheric Chemistry and Physics*, *11*, 10619–10636. http://dx.doi.org/10.5194/acp-11-10619-2011.
Curier, L., de Leeuw, G., Kolmonen, P., Sundstrom, Anu-Maija, Sogacheva, L., & Bennouna, Y. (2009). Aerosol retrieval over land using the (A)ATSR dual-view algorithm. In A. A. Kokhanovsky, & G. de Leeuw (Eds.), *Satellite aerosol remote sensing over land* (pp. 135–160). Chichester, UK: Praxis Publishing.
Damoah, R., Spichtinger, N., Forster, C., James, P., Mattis, I., Wandinger, U., et al. (2004). Around the world in 17 days — hemispheric-scale transport of forest fire smoke from Russia in May 2003. *Atmospheric Chemistry and Physics*, *4*, 1311–1321. http://dx.doi.org/10.5194/acpd-4-1449-2004.
de Leeuw, G. S., Kinne, J. F., Leon, J., Pelon, D., Rosenfeld, M., Schaap, P. J., Veefkind, B., Veihelmann, D. M., Winker, & von Hoyningen-Huene, W. (2011). Retrieval of aerosol properties. 536 pp. In J. P. Burrows, U. Platt, & P. Borrell (Eds.), *The remote sensing of tropospheric composition from space* (pp. 259–314). Berlin Heidelberg: Springer-Verlag978-3-642-14790-6. http://dx.doi.org/10.1007/978-3-642-14791-3.
Delworth, T. L., Ramaswamy, V., & Stenchikov, G. L. (2005). The impact of aerosols on simulated ocean temperature and heat content in the 20th century. *Geophysical Research Letters*, *32*, L24709. http://dx.doi.org/10.1029/2005GL024457.
Deuze, J. L., Breon, F. M., Devaux, C., Goloub, P., Herman, M., Lafrance, B., et al. (2001). Remote sensing of aerosols over land surfaces from POLDER-ADEOS-1 polarized measurements. *Journal of Geophysical Research*, *106*(D5), 4913–4926.
Diner, D. J., Martonchik, J. V., Kahn, R. A., Pinty, B., Gobron, N., Nelson, D. L., et al. (2005). Using angular and spectral shape similarity constraints to improve MISR aerosol and surface retrievals over land. *Remote Sensing of Environment*, *94*(2), 155–171.
Eck, T. F., Holben, B. N., & Reid, J. S. (1999). Wavelength dependence of the optical depth of biomass burning, urban, and desert dust aerosol. *Journal of Geophysical Research*, *104*(D24), 31,333–31,349.
Flowerdew, R. J., & Haigh, J. D. (1995). An approximation to improve accuracy in the derivation of surface reflectances from multi-look satellite radiometers. *Geophysical Research Letters*, *22*(13), 1693–1696.
Fröhlich, C., & Shaw, E. (1980). new determination of Rayleigh scattering in the terrestrial atmosphere. *Applied Optics*, *19*(11), 1773–1775.
Gatebe, C. K., King, M. D., Tsay, S. C., Ji, Q., Thomas, A. G., & Li, J. Y. (2001). Sensitivity of off-nadir zenith angles to correlation between visible and near-infrared reflectance for use in remote sensing of aerosol over land. *IEEE transaction on geoscience and remote sensing*, *39*(4), 805–819.
Govaerts, Y. M., Wagner, S., Lattanzio, A., & Watts, P. (2010). Joint retrieval of surface reflectance and aerosol optical depth from MSG/SEVIRI observations with an optimal estimation approach: 1. Theory. *Journal of Geophysical Research*, *115*(D02203). http://dx.doi.org/10.1029/2009JD011779.
Grey, W. M. F., North, P. R. J., Los, S. O., & Mitchell, R. M. (2006). Aerosol optical depth and land surface reflectance from multi-angle AATSR measurements: global validation and inter-sensor comparisons. *IEEE Transactions on Geoscience and Remote Sensing*, *44*(8), 2184–2197.
Heintzenberg, J., Tuch, T., Wehner, B., Wiedensohler, A., Wex, H., Ansmann, A., et al. (2003). Arctic haze over Central Europe. *Tellus*, *55B*, 796–807.
Henyey, L. C., & Greenstein, J. L. (1941). Diffuse radiation in the galaxy. *The Astrophysical Journal*, *93*, 70–83.
Herber, A., Thomason, L. W., Dethloff, K., Viterbo, P., Radionov, V. F., & Leiterer, U. (1996). Volcanic perturbation of the atmosphere in both polar regions :1991–1994. *Journal of Geophysical Research*, *101*(D2), 3921–3928. http://dx.doi.org/10.1029/95JD02462.
Hess, M., Koepke, P., & Schult, I. (1998). Optical properties of aerosols and clouds: The software package OPAC. *Bulletin of the American Meteorological Society*, *79*, 831–844.
Holben, B. N., Eck, T. F., Slutsker, I., Tanre, D., Buis, J. P., Setzer, A., et al. (1998). *Remote Sensing of Environment*, *66*, 1–16.
Hsu, N. C., Tsay, S. C., King, M. D., & Herman, J. R. (2004). Aerosol properties over bright reflecting source regions. *IEEE Transactions on Geoscience and Remote Sensing*, *42*(3), 557–569.
Hudson, S. R., Warren, S. G., Brandt, R. E., Grenfell, T. C., & Six, D. (2006). Spectral bidirectional reflectance of Antarctic snow: Measurements and parameterization. *Journal of Geophysical Research*, *111*(D18106). http://dx.doi.org/10.1029/2006JD007290.
Ichoku, C., Chu, D. A., Mattoo, S., Kaufman, Y. J., Remer, L. A., Tanre, D., et al. (2002). A spatio-temporal approach for global validation and analysis of MODIS aerosol products. *Geophysical Research Letters*, *29*(12). http://dx.doi.org/10.1029/2001GL013206.
Istomina, L. G., von Hoyningen-Huene, W., Kokhanovsky, A. A., & Burrows, J. P. (2009). Retrieval of aerosol optical thickness in arctic region using dual-view AATSR observations. *Proceedings of ESA Atmospheric Science Conference, Barcelona, 07.-11. Sept.2009. ESA SP-676*.
Istomina, L. G., von Hoyningen-Huene, W., Kokhanovsky, A. A., Schultz, E., & Burrows, J. P. (2011). Remote sensing of aerosol over snow using infrared AATSR observations. *Atmospheric Measurement Techniques*, *4*, 1133–1145.
Jacob, D. J., Crawford, J. H., Maring, H., Clarke, A. D., Dibb, J. E., Emmons, L. K., et al. (2010). The Arctic Research of the Composition of the Troposphere from Aircraft and Satellites (ARCTAS) mission design, execution, and first results. *Atmospheric Chemistry and Physics*, *10*, 5191–5212.
Kahn, R. & the MISR Team. (2008). http://www.espo.nasa.gov/arctas/docs/presentations/Kahn_MISR_Overview.pdf (accessed on 10 October 2012).
Kasten, J., & Young, A. T. (1989). revised optical air mass tables and approximation formula. *Applied Optics*, *28*, 22,437–22,4378.
Kaufman, Y. J., Tanre, D., Remer, L. A., Vermote, E. F., Chu, A., & Holben, B. N. (1997). Operational remote sensing of tropospheric aerosol over land from EOS moderate resolution imaging spectroradiometer. *Journal of Geophysical Research*, *102*(D14), 17051–17067. http://dx.doi.org/10.1029/96JD03988.
Key, J. R., Santek, D., Velden, C. S., Bormann, N., Thépaut, J. -N., Riishojgaard, L. P., et al. (2003). Cloud-drift and water vapor winds in the polar regions from MODIS. *IEEE Transactions on Geoscience and Remote Sensing*, *41*(2), 482–492.
Kim, Y., Hatsushika, H., Muskett, R. R., & Yamazaki, K. (2005). Possible effect of boreal wildfire soot on Arctic sea ice and Alaska glaciers. *Atmospheric Environment*, *39*(19), 3513–3520.
Kokhanovsky, A. A., Aoki, T., Hachikubo, A., Hori, M., & Zege, E. P. (2005). Reflective properties of natural snow: Approximate asymptotic theory versus in situ measurements. *IEEE Transactions on Geoscience and Remote Sensing*, *43*(7), 1529–1535.
Kokhanovsky, A. A., & de Leeuw, G. (Eds.). (2009). *Satellite aerosol remote sensing over land*. Berlin: Springer-Praxis978-3-540-69396-3 (388 pp.).
Kolmonen, P., Sundström, A. -M., Sogacheva, L., Rodriguez, E., Virtanen, T. H., & de Leeuw, G. (2012). Towards the assimilation of the satellite retrieved aerosol properties: the uncertainty characterization of AOD for the AATSR ADV/ASV retrieval algorithm. In preparation for submission to AMT.
Kondratyev, K. Y. (1969). *Radiation in the atmosphere*. New York and London: Academic Press.
Kondratyev, K. Y., & Varotsos, C. (1995). Atmospheric greenhouse effect in the context of global climate change. *Il Nuovo Cimento C*, *18*(2), 123–151. http://dx.doi.org/10.1007/BF02512015.
Kuzetzov, E. S. (1942). On the problem of approximate transfer equations in a scattering and absorbing medium. *Reports of Academy of Science, USSR 37, Nos, 7 and 8*.
Levenberg, K. (1944). A method for the solution of certain non-linear problems in least squares. *Quarterly of Applied Mathematics*, *II*(2), 164–168.
Levy, R. C., Remer, L., Mattoo, S., Vermote, E. F., & Kaufman, Y. J. (2007). Second-generation algorithm for retrieving aerosol properties over land from MODIS spectral reflectance. *Journal of Geophysical Research*, *112*(D13211). http://dx.doi.org/10.1029/2006JD007811.
Linke, F. (Eds.), (1956). Die Sonnestrahlung und ihre Schwauml, chung in der Atmosphere. In F. Linke, & F. Moeller, (Eds.), *Handbuch der Geopgyisk*, VIII, 1942–1956, Gebr. Borntraeger, Berlin.
Lu, L. H., & Bian, L. G. (2011). Progresses of research on polar meteorological sciences in china over the last third decades. *Chinese Journal of Polar Research*, *23*(1), 1–10.
Maignan, F., Bréon, F. M., & Lacaze, R. (2004). Bidirectional reflectance of Earth targets: Evaluation of analytical models using a large set of space borne measurements with emphasis on the hot spot. *Remote Sensing of Environment*, *90*(2), 210–220.
Martonchik, J. V., Kahn, R. A., & Diner, D. J. (2009). Retrieval of aerosol properties over land using MISR observations. *Satellite aerosol remote sensing over land* (pp. 267–268). Chichester, UK: association with Praxis Publishing.
Mei, L., Xue, Y., de Leeuw, G., Guang, J., Wang, Y., Li, Y., et al. (2011). Integration of remote sensing data and surface observations to estimate the impact of the Russian wildfires over Europe and Asia during August 2010. *Biogeosciences*, *8*, 3771–3791. http://dx.doi.org/10.5194/bg-8-3771-2011.
Painter, T. H., & Dozier, J. (2004). Measurements of the hemispherical-directional reflectance of snow at fine spectral and angular resolution. *Journal of Geophysical Research*, *109*(D18115). http://dx.doi.org/10.1029/2003JD004458.
Quinn, P. K., Shaw, G., Andrews, E., Dutton, E. G., Ruoho-Airola, T., & Gong, S. L. (2007). Arctic haze: current trends and knowledge gaps. *Tellus*, *59B*, 99–114.
Remer, L. A., Kaufman, Y. J., Tanre, D., Mattoo, S., Chu, D. A., Martins, J. V., et al. (2005). The MODIS aerosol algorithm, products, and validation. *Journal of the Atmospheric Sciences*, *62*(4), 947–973.
Remer, L. A., Tanré, D., & Kaufman, Y. J. (2006). Algorithm for Remote Sensing of Tropospheric Aerosol from MODIS: Collection 5, ATBD_MOD_02.pdf. http://modis.gsfc.nasa.gov/data/atbd/atmos_atbd.php.Nov.1 (accessed on 10/10/2011)
Remer, L. A., Wald, A. E., & Kaufman, Y. J. (2001). Angular and seasonal variation of spectral surface reflectance rations: implications for the remote sensing of aerosol over land. *IEEE transaction on geoscience and remote sensing*, *39*(2), 275–283.
Rodríguez, E., Toledano, C., Cachorro, V., de Leeuw, G., de Frutos, A., Gausa, M., et al. (2007). Comparison of aerosol optical properties at the sub-arctic stations ALOMAR-Andenes, Abisko and Sodankylä in late spring and summer 2007. *Atmospheric Research*, *107*, 20–30.
Rodríguez, E., Toledano, C., Cachorro, V. E., Ortiz, P., Stebel, K., Berjón, A., et al. (2011). Aerosol characterization at the sub-Arctic site Andenes (69°N, 16°E), by the analysis of columnar optical properties. *Quarterly Journal of the Royal Meteorological Society*, *138*(663), 471–482.
Saltelli, A., Ratto, M., Andres, T., Campolongo, F., Cariboni, J., Gatelli, D., et al. (2008). *Global sensitivity analysis*. The Primer: John Wiley & Sons.

Santer, R., Carrere, V., Dubuisson, P., & Roger, J. C. (1999). Atmospheric corrections over land for MERIS. *International Journal of Remote Sensing*, *20*, 1819–1840.

Shaw, G. E. (1995). The Arctic haze phenomenon. *Bulletin of the American Meteorological Society*, 2403–2413.

Shindell, D., & Faluvegi, G. (2009). Climate response to regional radiative forcing during the twentieth century. *Nature Geoscience*, *2*, 294–300. http://dx.doi.org/10.1038/ngeo473.

Stohl, A. (2006). Characteristics of atmospheric transport into the Arctic troposphere. *Journal of Geophysical Research*, *111*, D11306. http://dx.doi.org/10.1029/2005JD00.

Tang, J., Xue, Y., Yu, T., & Guan, Y. (2005). Aerosol optical thickness determination by exploiting the synergy of TERRA and AQUA MODIS. *Remote Sensing of Environment*, *94*, 327–334.

Toledano, C., Cachorro, V., Gausa, M., Stebel, K., Aaltonen, V., Berjón, A., et al. (2012). Overview of sun photometer measurements of aerosol properties in Scandinavia and Svalbard. *Atmospheric Environment*, *52*, 18–28.

Veefkind, J. P., de Leeuw, G., & Durkee, P. A. (1998). Retrieval of aerosol optical depth over land using two-angle view satellite radiometry during TARFOX. *Geophysical Research Letters*, *25*(16), 3135–3138.

Von Hoyningen-Huene, W., Freitag, M., & Burrows, J. P. (2003). Retrieval of aerosol optical thickness over land surface from top-of-atmosphere radiance. *Journal of Geophysical Research*, *108*(D9). http://dx.doi.org/10.1029/2001JD002018.

von Hoyningen-Huene, W., Yoon, J., Vountas, M., Istomina, L. G., Rohen, G., Dinter, T., et al. (2011). Retrieval of spectral aerosol optical thickness over land using ocean color sensors MERIS and SeaWiFS. *Atmospheric Measurement Techniques*, *4*, 151–171. http://dx.doi.org/10.5194/amt-4-151-2011.

Wagner, S. C., Govaerts, Y. M., & Lattanzio, A. (2010). Joint retrieval of surface reflectance and aerosol optical depth from MSG/SEVIRI observations with an optimal estimation approach: 2. Implementation and evaluation. *Journal of Geophysical Research*, *115*(D02204). http://dx.doi.org/10.1029/2009JD011780.

Wang, Y., Xue, Y., Li, Y. J., Guang, J., Mei, L. L., Xu, H., et al. (2012). Prior knowledge supported aerosol optical depth retrieval over land surface at 500 m spatial resolution with MODIS data. *International Journal of Remote Sensing*, *33*(3), 674–691.

Xue, Y., & Cracknell, A. P. (1995). Operational bi-angle approach to retrieve the Earth surface albedo from AVHRR data in the visible band. *International Journal of Remote Sensing*, *16*(3), 417–429.